The Astrophysical Journal, 753:105 (10pp), 2012 July 10 doi:10.1088/0004-637X/753/2/105

A PHYSICAL MODEL FOR SN 2001ay, A NORMAL, BRIGHT, EXTREMELY SLOW DECLINING TYPE Ia SUPERNOVA

E. Baron[1,2,3,4], P. Höflich[5], K. Krisciunas[6], I. Dominguez[7], A. M. Khokhlov[8], M. M. Phillips[9], N. Suntzeff[6], and L. Wang[6]

[1] Homer L. Dodge Department of Physics and Astronomy, University of Oklahoma, 440 W. Brooks, Rm 100, Norman, OK 73019-2061, USA; baron@ou.edu
[2] Hamburger Sternwarte, Gojenbergsweg 112, 21029 Hamburg, Germany
[3] Computational Research Division, Lawrence Berkeley National Laboratory, MS 50B-4206, 1 Cyclotron Rd, Berkeley, CA 94720, USA
[4] Physics Department, University of California, Berkeley, CA 94720, USA
[5] Department of Physics, Florida State University, Tallahassee, FL 32306, USA; pah@astro.physics.fsu.edu
[6] George P. and Cynthia Woods Mitchell Institute for Fundamental Physics & Astronomy, Department of Physics & Astronomy, Texas A&M University, 4242 TAMU, College Station, TX 77843, USA; krisciunas@physics.tamu.edu, suntzeff@physics.tamu.edu, lwang@physics.tamu.edu
[7] Department of Physics, Universidad de Granada C/ Bajo de Huetor 24 Aptdo 3004, ES 18071, Granada, Spain; inma@ugr.es
[8] Department of Astronomy and Astrophysics, University of Chicago, Chicago, IL, USA; ajk@oddjob.uchicago.edu
[9] Las Campanas Observatory, Casilla 601, La Serena, Chile; mmp@lcoeps1.lco.cl
Received 2011 December 21; accepted 2012 May 2; published 2012 June 19

ABSTRACT

We present a study of the peculiar Type Ia supernova 2001ay (SN 2001ay). The defining features of its peculiarity are high velocity, broad lines, and a fast rising light curve, combined with the slowest known rate of decline. It is one magnitude dimmer than would be predicted from its observed Δm_{15}, and shows broad spectral features. We base our analysis on detailed calculations for the explosion, light curves, and spectra. We demonstrate that consistency is key for both validating the models and probing the underlying physics. We show that this SN can be understood within the physics underlying the Δm_{15} relation, and in the framework of pulsating delayed detonation models originating from a Chandrasekhar mass, $M_{\rm Ch}$, white dwarf, but with a progenitor core composed of 80% carbon. We suggest a possible scenario for stellar evolution which leads to such a progenitor. We show that the unusual light curve decline can be understood with the same physics as has been used to understand the Δm_{15} relation for normal SNe Ia. The decline relation can be explained by a combination of the temperature dependence of the opacity and excess or deficit of the peak luminosity, α, measured relative to the instantaneous rate of radiative decay energy generation. What differentiates SN 2001ay from normal SNe Ia is a higher explosion energy which leads to a shift of the ^{56}Ni distribution toward higher velocity and $\alpha < 1$. This result is responsible for the fast rise and slow decline. We define a class of SN 2001ay-like SNe Ia, which will show an anti-Phillips relation.

Key word: supernovae: individual: SN 2001ay

Online-only material: color figures

1. INTRODUCTION

While some progress has been made in the understanding of the Type Ia supernova (SN Ia) phenomenon in recent years, there does not yet exist an agreed upon standard model of the supernova explosion that can explain normal SNe Ia (Branch et al. 2005, 2009). For cosmology, the brightness decline relation plays a key role (Phillips 1993; Phillips et al. 1999; Goldhaber et al. 2001). From theory, Δm_{15} is well understood: the light curves (LCs) are powered by radioactive decay of ^{56}Ni (Colgate & McKee 1969). More ^{56}Ni increases the luminosity and causes the envelopes to be hotter. Higher temperature means higher opacity and, thus, longer diffusion timescales and slower decline rates after maximum light (Höflich et al. 1996; Nugent et al. 1997; Umeda et al. 1999; Kasen et al. 2009). The existence of a Δm_{15} relation holds for virtually all scenarios as long as there is an excess amount of stored energy to be released (Höflich et al. 1996). Although the tightness of the relation can be understood within the framework of the single degenerate scenario and spherical models (Höflich et al. 1996, 2002, 2010), it falls apart when taking into account burning instabilities during the deflagration phase (Kasen et al. 2009). This difficulty and the observation of a set of extremely bright SNe Ia may lend support for double degenerate (DD) scenarios (Tutukov & Yungelson 1979; Iben & Tutukov 1984; Webbink 1984) with progenitors well above the Chandrasekhar mass (Howell et al. 2006; Scalzo et al. 2010; Taubenberger et al. 2011; Howell 2011). We note, however, that the inferred brightness depends on a unique relation between the ^{56}Ni mass $M_{\rm Ni}$, and the intrinsic color: $B-V$ at maximum light. At least in a few cases, the apparent brightness can be understood within the framework of $M_{\rm Ch}$ mass white dwarfs (WDs) with intrinsically red color (Quimby et al. 2006).

Additionally, some progress has been made in understanding variations among the groups, with suggestions that some of the spectral diversity is due to metallicity, central density, and asymmetries (Höflich et al. 1998, 2010; Lentz et al. 2000; Maeda et al. 2010; Maund et al. 2010). The nature of the progenitor system is also controversial, with recent work on rates and the delay time distribution favoring the DD scenario (Yungelson & Livio 1998, 2000; Maoz 2008; Ruiter et al. 2009; Maoz et al. 2010, 2011; Mennekens et al. 2010; Ruiter et al. 2011). Nevertheless, theoretical work continues to favor the single degenerate scenario, with some contribution of DD scenario (Höflich & Khokhlov 1996; Saio & Nomoto 1998; Woosley & Weaver 1986; Mochkovitch & Livio 1990; Saio & Nomoto 1985; Shen et al. 2012).

Despite the uncertainties in theory, most of the known SNe Ia obey the brightness decline relation. The LCs are self-similar within ±0.3 mag (Goldhaber & Perlmutter 1998; Riess et al.

1999). Deviations of this order can be expected from variations of the progenitor (Höflich et al. 1998; Brachwitz et al. 2000; Thielemann et al. 2003; Seitenzahl et al. 2011). The stretching method works for both the local and high-z samples (Perlmutter et al. 1999; Riess et al. 1998). The self-similarity holds even for supernovae for which super-Chandrasekhar mass progenitors have been suggested.

The subject of this paper, SN 2001ay, shows that nature is even more diverse (Krisciunas et al. 2011). From the redshift of the host galaxy IC4423 (Freedman et al. 2001), the distance modulus $\mu = 35.55 \pm 0.1$ is well known. The reddening in our Galaxy is found to be $E(B-V) = 0.026 \pm 0.006$ mag, and interstellar absorption in Na I suggests low reddening in the host galaxy of about $E(B-V) = 0.072 \pm 0.008$ mag (Krisciunas et al. 2011). Together with the observed magnitude, the intrinsic brightness at maximum light is $M_V = -19.17$ mag with a $B-V$ color of -0.02 mag, which is comparable with typical core-normal supernovae.

However, the LC shape is unlike other SNe Ia: its measured decline rate of $\Delta m_B = 0.68$ is slower than any known SNe Ia, combined with a fast rise of some 16 days (Krisciunas et al. 2011). Based on its Δm_{15}, SN 2001ay should be brighter than observed by about 1 mag. Moreover, the line widths near maximum light put it solidly in the broad-line class of SNe Ia.

We show that SN 2001ay can be understood with the same physics underlying the Δm_{15} relation, and in the framework of parameterized pulsating delayed detonation (PDD) models similar to SN 1990N (Khokhlov et al. 1992), but with an unusual progenitor star. We consistently treat the explosion, LCs, and spectra (Höflich 1995). We show that consistent models reproduce the observed LCs and spectra reasonably well. Furthermore, we show that inconsistent calculations lead to spectral features which would lead to rejection of the explosion model. Finally, we summarize our findings and discuss possible implications for the understanding of SNe Ia and cosmology.

2. MOTIVATION FOR OUR MODEL FOR SN 2001ay

For our models, an understanding of the brightness decline relation is important. The Phillips relation (Phillips 1993; Phillips et al. 1999) provides an empirical link between peak brightness and decline of the LC after maximum. Most SNe Ia fall within 0.2 mag of this relation.

As discussed in the Introduction, the Δm_{15} relation can be understood as an opacity effect if energy in stored energy is available in excess of the instantaneous radioactive decay (Höflich et al. 1996; Nugent et al. 1997; Umeda et al. 1999; Kasen et al. 2009). The latter is a key to understand SN 2001ay. We will discuss that while the second condition is valid in most scenarios for SNe Ia, it is not guaranteed.

For our discussion, a useful quantity is the relation between instantaneous energy deposition by radioactive decay and the brightness at maximum:

$$L_{\rm bol}(t_{\rm max}) = \alpha \dot{S}(t_{\rm max}),$$

where α accounts for the fact that some of the γ-ray energy deposited prior to maximum light can be stored in the thermal energy and trapped radiation energy which cannot escape faster than a diffusion time. In a typical delayed detonation model the value of α is about 1.2 (Khokhlov et al. 1993; Höflich & Khokhlov 1996).

The role of the opacity condition can be seen from Arnett's analytic solution (Arnett 1980, 1982), which also provides further insights. Constant opacity in a polytropic model with homogeneous energy input does not produce a brightness decline relation. In this model, energy balance between radioactive decay and adiabatic expansion and cooling cancel exactly in a radiation dominated regime with pure geometrical dilution. At maximum, the ratio between maximum brightness and instantaneous energy input is $\alpha = 1$. Pinto & Eastman (2000) reconsidered Arnett's one-zone models and confirmed previous explanations. Declining opacity provide extra energy at maximum light because it accelerates the recession of the "photosphere" (Höflich et al. 1993) and results in a positive brightness decline relation in this case.

However, even an effective opacity declining with temperature may result in an anti-Δm_{15} relation, because Δm_{15} depends both on the opacity effect and the excess energy available. For example, the pure detonation model DET1 has an $\alpha \approx 0.73$ and Δm_{15} of 1.37 mag. In contrast, another pure detonation model DET2 has an $\alpha \approx 1.2$ and $\Delta m_{15} \approx 1.7$ (Khokhlov et al. 1993; Höflich & Khokhlov 1996). In DET1, the high central density leads to significant electron capture in the central region producing a ^{56}Ni free core. In contrast, lower central densities in DET2 produce ^{56}Ni in the center, and less ^{56}Ni in the outer region. In both models, the density structure is close to similar polytropes but the ^{56}Ni distribution is shifted outward and inward, respectively. The differences in α can be understood in terms of the deviation from Arnett's one-zone model with a flat ^{56}Ni distribution in mass. In DET1, this distribution is shifted outward leading to an increased escape probability of γ-rays and greater expansion work which leads to reduced α. In DET2, the shift of the ^{56}Ni distribution inward leads to a larger value of α.

From the above discussion, it is obvious that a narrow Δm_{15} relation requires similar abundance patterns and ^{56}Ni distributions for a given $M_{\rm Ni}$. The theoretical relation $\Delta m_{15}(M_{\rm Ni})$ depends on the explosion scenario. Self-similarity in the LCs requires a self-similar transformation between models of differing brightness. Within the delayed-detonation scenario, $M_{\rm Ni}$ depends mostly on the pre-expansion during the deflagration phase, since if the density is too high neutron-rich iron-group elements will be produced. However, as the nickel mass drops out of the standard 0.5–0.6 $M_\odot$ range, the ^{56}Ni distribution shifts inward with decreasing $M_{\rm Ni}$. This produces a $\Delta m_{15}(M_{\rm Ni})$ relation which is in agreement with observations (Höflich et al. 2002). For core-normal SNe Ia, the temperature and, with it the opacity, remains high well after maximum light, leading to a "shallow" $\Delta m_{15}(M_{\rm Ni})$. Below a certain $M_{\rm Ni}$, the nickel is very centrally condensed (there is no nickel hole) and the opacity drops rapidly soon after maximum leading to a steep $\Delta m_{15}(M_{\rm Ni})$ relation. In the case of fast decliners ^{56}Ni is only produced during the deflagration phase.

3. SCENARIOS FOR SN 2001ay

3.1. Models with an Increased Mass

SN 2001ay was suggested to fall within the class of "Super-Chandra" mass SNe Ia. Obviously, SN 2001ay does not obey the standard Δm_{15} relation. Within the framework of the empirical Δm_{15} relation, SN 2001ay should be brighter than observed by roughly 1.0 mag which can be ruled out (see Figure 10 of Krisciunas et al. 2011). In fact, compared to the putative super-Chandrasekhar SNe Ia, 2007if (Scalzo et al. 2010; Yuan et al. 2010) and SN 2009dc (Yamanaka et al. 2009; Tanaka et al. 2010; Silverman et al. 2011; Taubenberger et al. 2011) estimates of

$M_{\rm bol}$ at maximum light differ by about 1 mag. Estimates for the brightness of SN 2001ay imply 0.5 $M_{\rm Ni}$ (Krisciunas et al. 2011). We need an increase of the diffusion timescales by a factor of two from Δm_{15} of 1.25 for typical SNe Ia (Phillips et al. 1999) to $\Delta m_{15} = 0.68$. The diffusion times scale as, $t_{\rm diff} \propto \tau^2 \propto M^2$ and, for homologous expansion, $\tau \propto t^{-2}$. If we assume $M_{\rm Ch}$ for normal SNe Ia, this would imply a progenitor mass of 2 $M_\odot$ which is super-Chandra and in fact typical of the mass suggested for mergers, but then one must explain why some super-Chandras are extra bright and SN 2001ay is not.

A stronger argument against a high mass progenitor comes from the rise time to decline ratio. SN 2001ay rises quickly to maximum, whereas an increased timescale would unavoidably produce a slow rise to maximum light.

3.2. The Case for an $M_{\rm Ch}$ Mass WD with a Faster Expansion Rate

Here, we suggest another scenario outside the "classical" regime for SNe Ia, but within the delayed-detonation scenario of Chandrasekhar mass WD progenitors. To reproduce SN 2001ay, we require a fast rising LC followed by a decline slower than the slope of the instantaneous radioactive decay. We can produce models with $\alpha < 1$. This requires a model with ^{56}Ni shifted to high velocities. Since eventually, the luminosity is given by the rate of instantaneous energy deposition, such a model will show a slow decline by construction.

4. RESULTS

4.1. Explosion Models and Light Curves

We describe how a change of parameters can transform the results from that given by normal LCs to that of SN 2001ay, within the same physical picture.

Even in the absence of a well agreed upon model for SNe Ia most of the basic observational properties, that is, LCs and spectra, of core-normal SNe Ia can be understood within the framework of thermonuclear explosions of Chandrasekhar mass WDs and, in particular, the delayed-detonation scenario (Khokhlov 1989) which provides a natural explanation for the wide variety and range of the ^{56}Ni production. To first order, the amount of ^{56}Ni produced in the explosion depends on the pre-expansion of the WD during the deflagration phase, in which spherical models can be parameterized conveniently by the density at which the transition between deflagration to detonation occurs. For a recent review of the relation between observational properties and the underlying physical model, see, for example, Höflich (2006).

We base our analysis on a spherical explosion model within the framework of the PDD scenario. Our goal is to construct a model with reduced α and short diffusion timescales. We seek to obtain our goals by increasing the expansion ratio and shifting of the ^{56}Ni distribution to higher velocity.

4.1.1. Explosion Models

The spherical explosion model has been constructed to allow fits of optical LCs and spectra of SN 2001ay.

Within the DD scenario, the free model parameters are (1) the chemical structure of the exploding WD, (2) its central density, ρ_c at the time of the explosion, (3) the description of the deflagration front, and (4) the layer at which the transition from deflagration to detonation occurs.

As a reference, we started from the delayed detonation model 5p0y25z22.25, which has been found to be a good starting point for core-normal SNe Ia, with respect to both spectra and LCs (Domínguez et al. 2001; Höflich 2002; Quimby et al. 2006; Höflich et al. 2010). This base model originates from a star with a main-sequence mass of 5 $M_\odot$ and solar metallicity. Through accretion, the C+O core of the star has grown close to the Chandrasekhar limit. At the time of the explosion of the WD, its central density is 2.0×10^9 g cm^{-3} and its mass is close to 1.37 $M_\odot$. The transition density $\rho_{\rm tr}$ has been identified as the main factor which determines the ^{56}Ni production and, thus, the brightness of SNe Ia (Höflich 1995; Höflich et al. 1995, 2002; Iwamoto et al. 1999). The transition density $\rho_{\rm tr}$ from deflagration to detonation is 25×10^6 g cm^{-3}.

For SN 2001ay, we tuned the parameters. The reference model has been modified as follows. We reduced the central density, ρ_c to 1×10^9 g cm^{-3}, which decreased the potential energy, as always, and thus, increased the radius of the WD by ≈30% to 2320 km, and we increased the C/O ratio in the former He-burning core ($M < 0.56\ M_\odot$) to 4. Both modifications increase the explosion energy to 1.69×10^{51} erg (1.69 foe), leading to a more rapid expanding envelope, increasing the rate of geometrical dilution, and shifting the ^{56}Ni to higher velocity. These effects are responsible for both the fast rise and slower decline of SN 2001ay.

In classical DD models, the deflagration to detonation transition (DDT) occurs in a WD already unbound during the deflagration phase (Khokhlov 1989; Yamaoka et al. 1992). In contrast, in pulsating delayed models, PDD, the WD remains bound after the deflagration phase, and the DDT occurs during pulsation (Khokhlov 1993; Hoflich et al. 1995). Other authors have suggested variations on the PDD (Ivanova et al. 1974; Bravo & García-Senz 2006, 2009; Baron et al. 2008; Bravo et al. 2009), but here when we discuss the PDD model, we specifically refer to the model of Khokhlov (1993). Reducing the burning rate during the deflagration phase moves the model from the DD to the PDD regime in which the WD is bound at the end of the deflagration phase. We artificially reduced the Atwood number, which we approximate as a constant independent of density and composition (see the Appendix) from 0.2 to (0.14, 0.12, 0.10) for the series PDD_11a–c which all undergo weak pulsation—producing LCs with rise times between 14 and 16 days with a slow decline from maximum. The best fit to the observations is given by PDD_11b. Its details are described below. While some of the observed trends that we find with the PDD model may be obtained in a three-dimensional DD model, including the effects of rotation, exploring such models is beyond the scope of this work. We mention results from PDD_11a/c below when needed.

The density and abundance structure of PDD_11b is given in Figures 1 and 2. The pulsation leaves a shell of ≈0.06 $M_\odot$ of unburned C/O (with C/O ∼1, only the region of central helium burning has enhanced C/0), and 0.51 $M_\odot$ of ^{56}Ni. For PDD models, mixing during the pulsation may occur. In contrast to previous pulsating models (Hoflich et al. 1995; Höflich & Khokhlov 1996), we did not assume full mixing during the pulsation, but instead mixing was limited to one scale height from the position of the burning front during the pulsation. The mixed region between burned matter forms the layer where the detonation is born. As a result, the density and chemical structure are similar to spherical DD models and consistent with late time line profiles and SN remnants. We abandoned full mixing in order to preserve the inner, unmixed region as required by late time line profiles and the imaging of the supernova remnant S Andromedae (Höflich et al. 2004; Motohara et al.

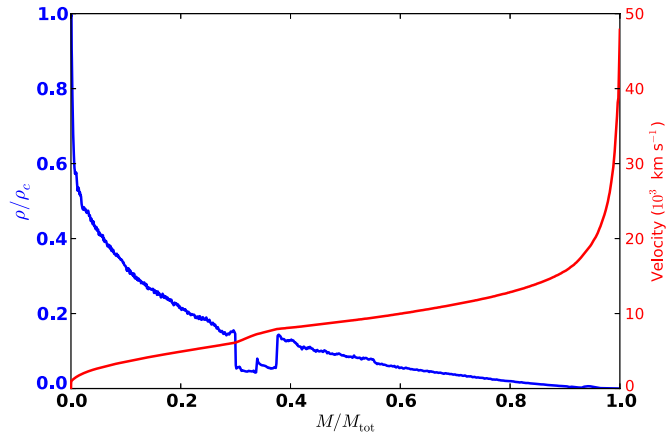

Figure 1. Density and velocity as a function of mass for model PDD_11b.
(A color version of this figure is available in the online journal.)

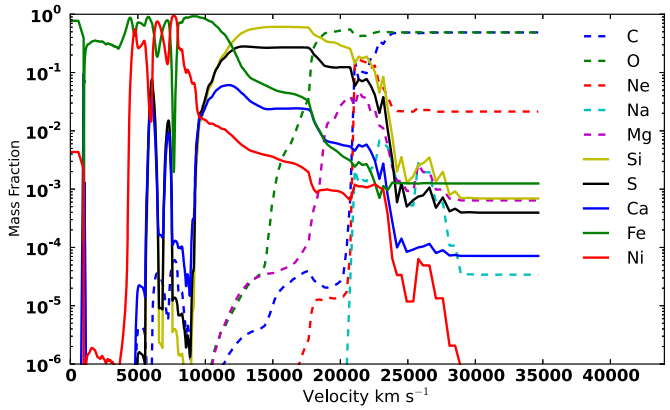

Figure 2. Abundances of stable isotopes as a function of the expansion velocity for model PDD_11b.
(A color version of this figure is available in the online journal.)

2006; Fesen et al. 2007; Gerardy et al. 2007; Maeda et al. 2010). Our models leave some unburned C/O. All modifications combined result in broader lines. We note that our model is highly parameterized. First, the deflagration phase depends critically on the initial condition and as discussed above, the problem of how to suppress strong mixing is still unsolved, though it may be related to high magnetic fields (Penney & Höflich 2012). Second, the amount of mixing will depend on Rayleigh–Taylor instabilities during the pulsation and possibly, rotation induced sheer instabilities.

4.1.2. Light Curves

Let us examine the formation of the LCs and the comparison with SN 2001ay. First, consider the energy input by γ-rays, positrons, and adiabatic cooling due to expansion. We contrast PDD_11b with our reference model. Both have a similar structure with respect to the chemical layering and, thus, similar opacities. Due to the higher explosion energy, the expansion rate of the inner layers is larger by about 25%–30%. PDD_11b shows an increased energy loss due to expansion work. The opacities for γ's depend only on the mass column height, τ_M, and the electron/nucleon ratio which is close to 0.5. τ_M scales as $v \times t^{-2}$ resulting in a 50% lower optical depth due to the higher velocity. The normalized energy deposition and escape fractions of γ-rays are shown in Figure 3. The high expansion rate results in strong heating by γ-rays in the outer region and a higher escape probability for γ-rays. Between 10 and 25 days, PDD_11b has an escape fraction larger than that of the reference model by about a factor of two.

In Figure 4, we give a comparison between LCs of PDD_11b and the reference model. PDD_11b rises faster and is brighter at early times. The higher escape of γ-rays and the increased expansion work leads to $\alpha < 1$ and, therefore, a lower peak relative to the rate of instantaneous γ-ray input. The second ingredient reducing the value of α is the opacity difference between optical photons and γ-rays. They are 0.1–0.2 and $1/35$ cm^2 g^{-1}, respectively. γ-rays leak into the center where the energy is trapped without contributing to the LC at maximum (Figure 3).

We therefore have a deficit in luminosity (with respect to the instantaneous γ-ray deposition rate), and the optical LCs approaches $\dot{E}_\gamma$ "from below." The same opacity mechanism responsible for the regular brightness decline relation results in an "anti-Phillips" relation. More ^{56}Ni and with it, larger opacities will lead to steeper declines.

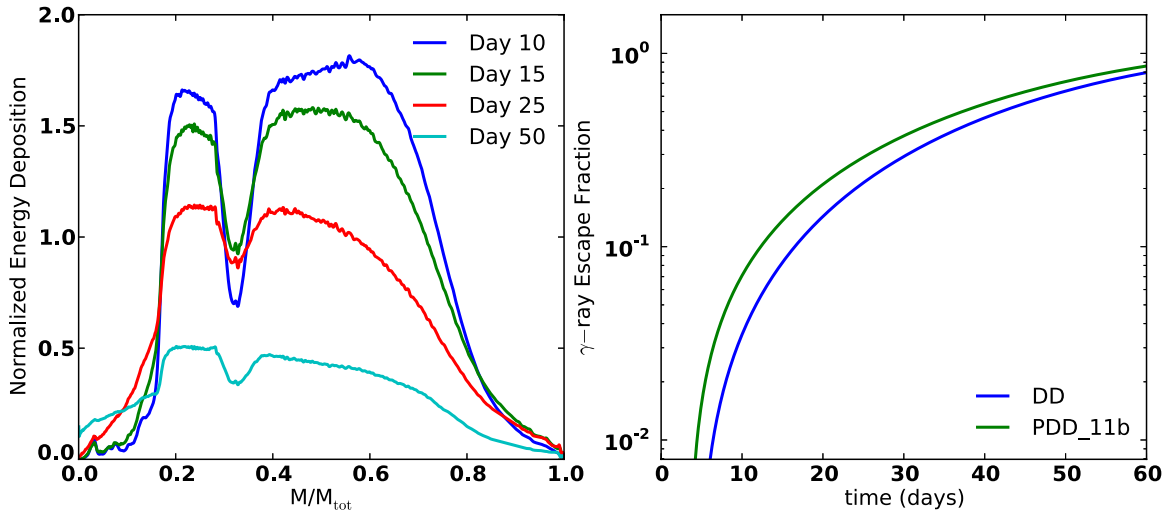

Figure 3. Normalized energy deposition by γ-ray and positrons in PDD_11b (left), and the escape fraction for PDD_11b and the reference model (right).
(A color version of this figure is available in the online journal.)

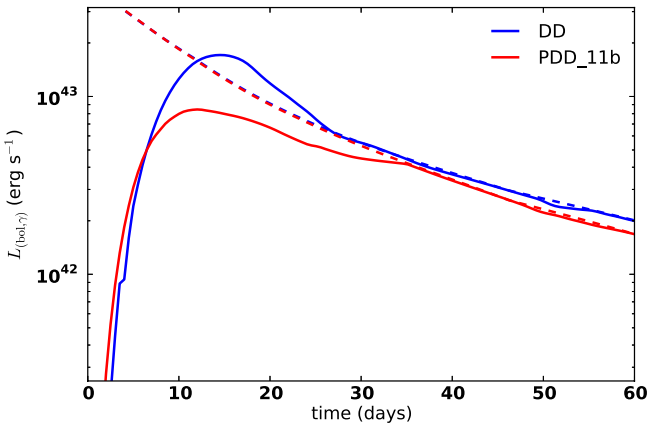

Figure 4. Instantaneous deposition rate due to radioactive decay (dashed) and bolometric luminosity (solid) for PDD_11b, a pulsating model with a carbon-rich core, and a "classical" DD model. The light curve of the DD model has been uniformly shifted by −0.037 dex and the light curve and γ-ray deposition of the PDD_11b model have been uniformly shifted by +0.05 dex to better illustrate the variation of the gradients.

(A color version of this figure is available in the online journal.)

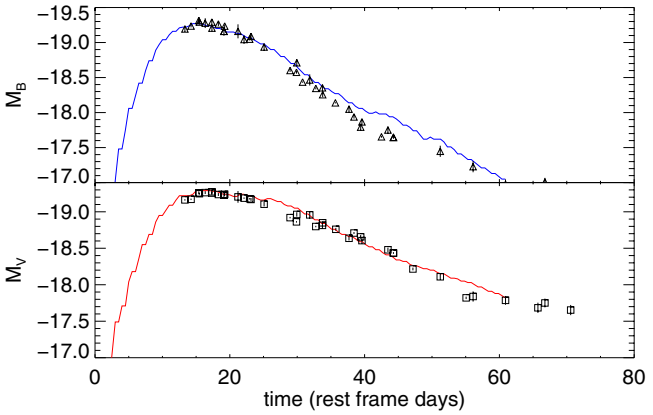

Figure 5. B and V LCs of SN 2001ay (Krisciunas et al. 2011) in comparison with theory. The comparison between SN 2001ay and PDD_11b in B (upper) and V (lower) as a function of time since maximum light in the V band. The model light curves have been corrected for reddening and redshift. We assume a distance modulus $m - M$ of 35.55 mag, and following Krisciunas et al. (2011), we take $A_V = 0.253$ and $A_B = 0.35$. The data include the photometric errors.

(A color version of this figure is available in the online journal.)

4.1.3. Comparison to SN 2001ay

In Figure 5, the theoretical LCs in B and V are compared with the observations. The agreement is reasonable, and they meet the brightness limit imposed by the early non-detection in R. The theoretical B and V have been corrected for the redshift z of the host galaxy. As discussed in the Introduction, the distance modulus of the host galaxy is 35.5 ± 0.1 mag, and the galactic foreground extinction $E(B - V) = 0.026$ mag. Krisciunas et al. (2011) use a reddening of the host galaxy of $E(B - V) = 0.072$ mag with an R_V of 3.1 and 2.4 for the Galaxy and host galaxy, respectively, giving $A_V = 0.253$ mag. Using our theoretical color, $(B - V)_{\max} = 0.0$ mag, and from an optimized fit, we find the host galaxy reddening $E(B - V) = 0.02$ mag with a global $R_V = 3.1$ for a total extinction $A_V = 0.144$ mag.

4.2. Spectral Analysis

Based on the explosion models, γ-ray transport, and LCs, we analyzed the spectrum of SN 2001ay at maximum light using the NLTE-code PHOENIX (see the Appendix).

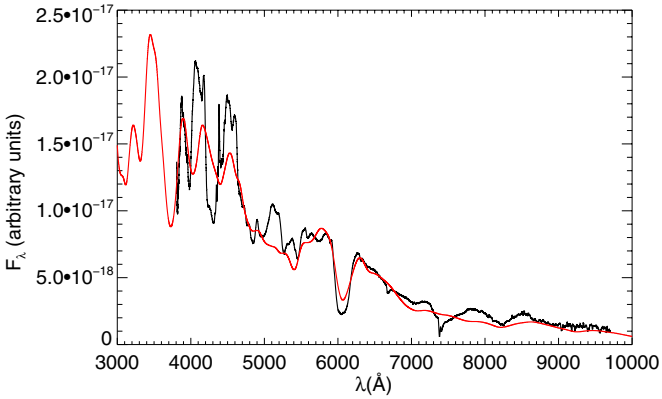

Figure 6. Synthetic spectrum at day 16 of PDD_11b in comparison with maximum spectrum of SN 2001ay. The density and abundance structure and the energy input by radioactive decay are taken from the explosion and light curve calculation (Figures 2, 3, and 5). Roughly consistent with the light curve, M_V was taken to be −19.07 mag, we have assumed standard reddening $R_V = 3.1$ and $E(B - V) = 0.096$.

(A color version of this figure is available in the online journal.)

We use the density, abundance structure, and γ-ray and positron deposition given by the explosion models and LC calculations. For the reddening and distance modulus, we use the values found from our LC fit. For the redshift, we use $z = 0.030244$. Converged models required 256 optical depth points.

For a consistent absolute M_V magnitude of −19.1 mag, the resulting synthetic spectrum is compared to the spectrum observed at maximum light in Figure 6. The continuum colors are well reproduced. The synthetic value of $B - V = -0.06$ mag, roughly consistent with 0 mag of SN 2001ay. In order to avoid the complications of two dust populations that was assumed by Krisciunas et al. (2011), we have taken $E(B - V) = 0.096$ and $R_V = 3.1$, so our reddening is a bit "bluer" that was assumed in the LC comparison, but it is well within the 0.1 mag error of the photometry.

The spectrum is dominated by single ionized lines of S II, Si II, Ca II, Fe II, Co II as well as blends of doubly ionized species in the blue. The synthetic and observed spectra show good agreement. The Doppler shifts of lines from elements undergoing incomplete oxygen burning include Si II λ6355, Si II λ5972 and S II λ5468 and λ5654, and the Ca II H+K and the IR triplet are reasonably well reproduced within 10, 20, and 30 Å, respectively, which corresponds to a velocity shift of 500–1000 km s^{-1} at the measured velocity of 14,400 km s^{-1}. The strength of the absorption components agrees well. A large number of weak lines form the quasi-continuum in the near IR. The feature due to blends of Fe II/Co II/Ni II which could possibly be misidentified as due to C II 6580 is reasonably strong, but the feature does not agree with the absorption notch identified as C II by Krisciunas et al. (2011). However, the evidence for C II claimed in Krisciunas et al. (2011) is stronger than warranted based on the analysis that were done for that paper (R. Thomas 2012, private communication). Some disagreement is evident. The S II W at about 5000 Å, blended with other lines, and the Si II λ5970 line are too weak. In the red, the Ca IR triplet is too weak, as is the O I λλ7773 line, which is, however, severely contaminated by Telluric absorption. The lack of O I is an indication that the outer part of our model is not correct, either in density structure or due to temperature effects.

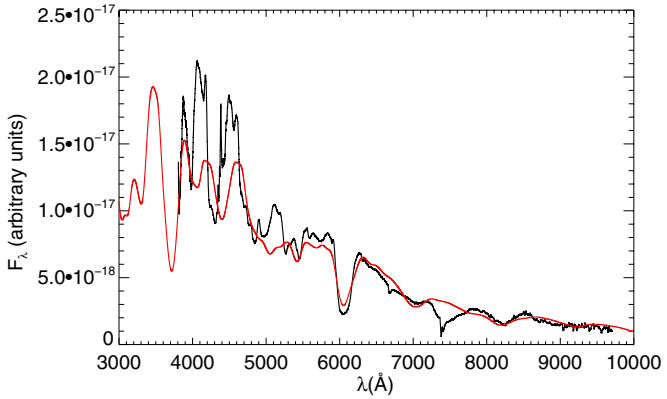

Figure 7. Same as Figure 6, but dimmer by 0.1 mag, i.e., M_V of −18.92 mag.
(A color version of this figure is available in the online journal.)

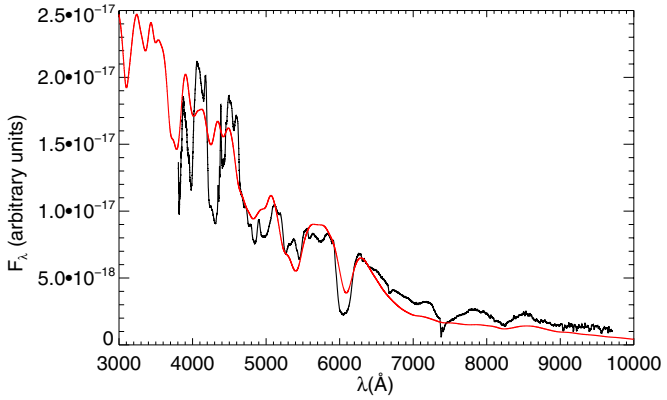

Figure 8. Same as Figure 6, but brighter by 0.15 mag, i.e., M_V of −19.23 mag.
(A color version of this figure is available in the online journal.)

To probe the importance of consistency and the sensitivity of the spectra, we calculated a series of maximum light spectra which are underluminous and overluminous, with M_V = (−18.92,−19.23,−19.35,−19.45) mag.

At +0.1 mag (Figure 7), the $B-V$ color becomes 0.03 mag. The Si II λ6355 line is well fit and the Ca II IR triplet is relatively well reproduced. In the blue, Co II lines dominate and a Co II line at 7400 Å appears. The feature at 6500 Å is weaker. The Doppler shift of the Si II and S II remains in good agreement because they are formed within the region of incomplete oxygen burning which produced nearly constant abundances due to burning in quasi-statistical equilibrium (QSE) conditions (Figure 2).

At −0.15 mag (Figure 8), $B-V$ equals −0.11 mag, but is clearly a little bit too blue as can be seen in the red part of the spectrum. However, the Si II λ5970 feature is too weak and S II lines are still significantly too weak. The Ca II IR triplet is much too weak. In the blue, Fe II lines are stronger and the fit is somewhat better. This could imply that the model should have had an initial metallicity somewhat higher, which would create more Fe II at the expense of Co II (from radioactive nickel).

At −0.25 mag (Figure 9), the spectrum becomes too blue, $B-V=-0.08$ mag, and the UV flux becomes too large. The Si II and S II lines are still significantly too weak and the IR flux is too low. The Ca H+K line is now too weak.

At −0.35 mag (Figure 10), the spectrum is much too blue, $B-V=-0.07$ mag and the Ca II features are completely absent. The Si II and S II features are now much too weak.

Figure 11 shows the model fit to the observed *Hubble Space Telescope* (*HST*)+Keck spectrum of April 29. The Si II line is

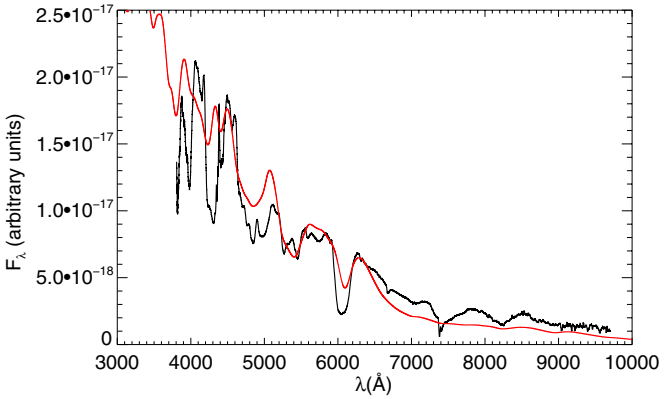

Figure 9. Same as Figure 6, but brighter by 0.25 mag, i.e., M_V of −19.35 mag.
(A color version of this figure is available in the online journal.)

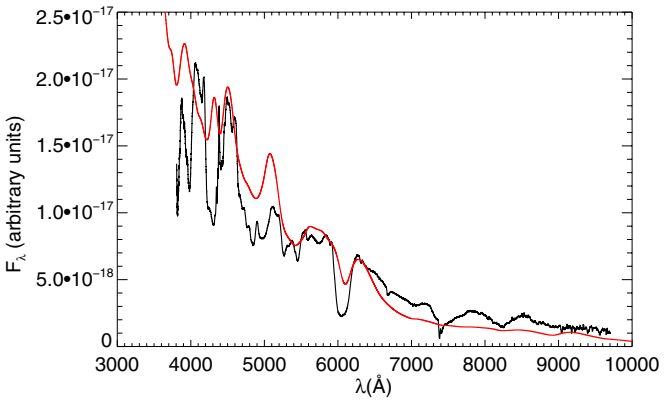

Figure 10. Same as Figure 6, but brighter by 0.35 mag, i.e., M_V of −19.45 mag.
(A color version of this figure is available in the online journal.)

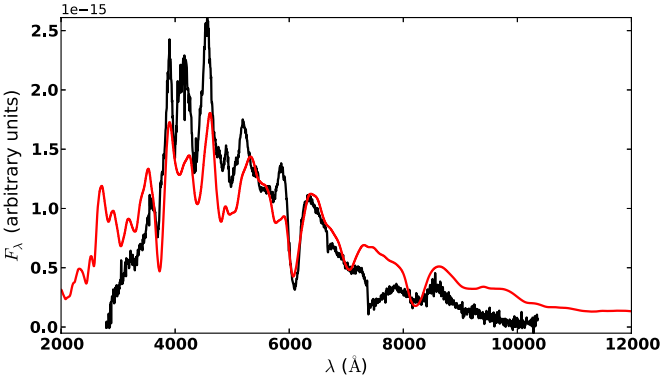

Figure 11. Synthetic spectrum (red) for 23 days after explosion compared with the observed spectrum obtained on 2001 April 29, from both *HST* and Keck. M_V is −18.97 mag and $B-V=0.43$.
(A color version of this figure is available in the online journal.)

very nicely fit, the S II "W" is well fit, although the blue line is a bit stronger in the model than in the observed spectrum. The rest of the blue is reasonably well fit, although the flux is about a factor of two too high in the UV, which may be an indication of the need for a higher metallicity, which would produce more line blanketing and reduce the UV flux. Both the Ca H+K and IR triplet are reasonably well fit, and the Co II + Fe II + Mn II feature at about 7350 Å is a bit too strong. The O I λλ7773 line is much too weak. Figure 12 shows the model fit for a somewhat brighter model $M_V=-19.22$ and $B-V=0.22$, still a bit too red, but the line features fit similarly well to the redder case.

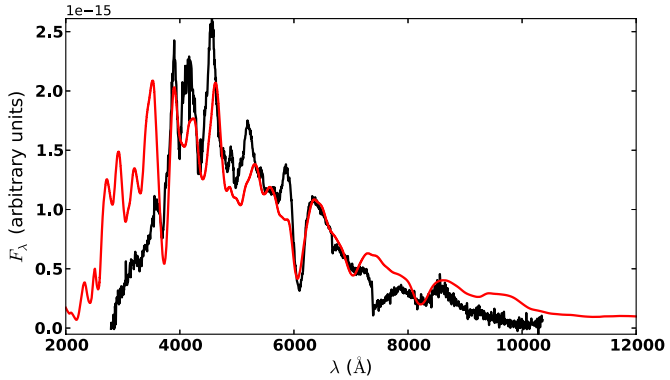

Figure 12. Same as Figure 11, but $M_V = -19.22$ mag and $B - V = 0.22$.
(A color version of this figure is available in the online journal.)

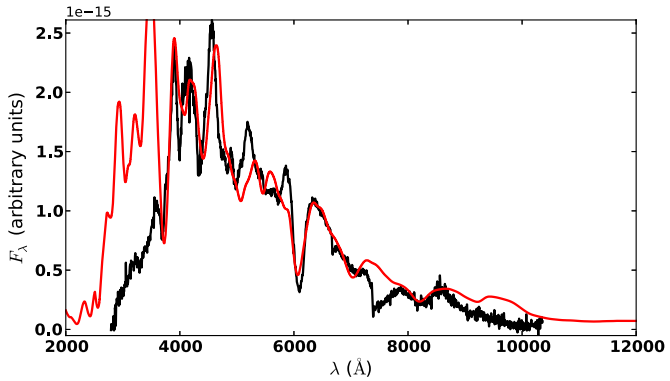

Figure 13. Same as Figure 11, but $M_V = -19.4$ mag and $B - V = 0.10$.
(A color version of this figure is available in the online journal.)

Figure 13 shows the model fit for a somewhat brighter model $M_V = -19.40$ and $B - V = 0.10$, a bit too bright, but about the right color. Again, the too high UV and the weak O I line are indications that the outer structure of our model is not quite correct, which could be due to primordial metallicity or our assumptions about mixing in the PDD.

Obviously, spectral synthesis is a very sensitive tool to probe the structure and luminosity on a level of $\Delta M_V \approx 0.1$ mag. Variations in excess of $\Delta M_V \approx 0.2$ lead to spectral fits which would lead to a rejection of even a valid, underlying explosion model. We note that our best fits give a "correct" velocity shift of, e.g., the Si II feature because, in PDD_11b, it is formed in the region of QSE for the Si/S group. Consistent treatment of explosion, LCs, and spectral formation is important. However, spectra lines are sensitive to both temperature effects and line blending and even a strong line like Si II λ6355 is not unblended. One can see a small blueward shift between Figures 6 and 11. Figure 14 shows the Si II λ6355 feature in velocity space, where two models at the same epoch (April 29) are plotted along with the data. The cooler model has an absorption minimum that is bluer than that of the hotter model and both are a bit bluer than the observed spectrum, although the noise in the spectrum makes a determination of the minimum a bit difficult.

In turn, LCs are mostly sensitive to the inner region and the large number of weak lines. Both in the LC and spectral calculation, $B - V$ is consistent, namely 0 and −0.06 mag. Only spectra show that the Si II line is too weak.

As discussed above, spherical models inherently suppress mixing by instabilities due to the deflagration phase at the inner layers, and the interaction between shells and the outer layers during the acceleration phase.

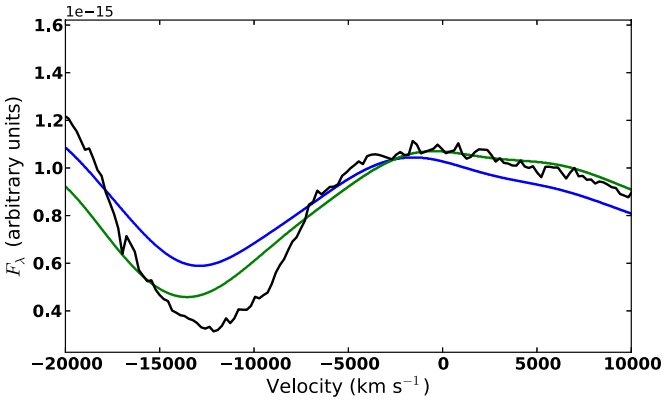

Figure 14. Si II λ6355 feature for 23 days after explosion compared with the observed spectrum obtained on 2001 April 29 (black) with the model shown in Figure 13 (green) and a somewhat hotter model (blue). The blueward shift in the absorption is clearly a temperature effect and is also due to blending.
(A color version of this figure is available in the online journal.)

Spectral analysis requires underlying models which are consistent including the luminosity. Then, however, they allow the study of secondary effects of individual spectral features.

5. DISCUSSION AND CONCLUSION

The peculiar Type Ia SN 2001ay is an important milestone for our understanding of the explosion, LCs, and spectra. Even with its extremely unusual LC shape and spectral features, we showed that it still can be accommodated within the framework of the explosion of a Chandrasekhar mass WD.

Although it does not follow the Δm_{15} relation, the LC can be reproduced within the physics of normal SNe Ia, and in the framework of PDD models. In our models, the key difference is a high, 80% carbon mass fraction, rather than the 15%–20% carbon mass fraction usual for stellar central He burning. The size of the carbon rich core is 0.56 $M_\odot$. The excess of carbon coupled with a lower central density of the initial WD results in an increase of the final kinetic energy by about 40% and, in turn, shifts the distribution of ^{56}Ni to larger velocities. These modifications are responsible for both the LC characteristics and the broad spectral features.

The peculiar LC shape is a consequence of the shift of the ^{56}Ni distribution in velocity space and higher rate of central expansion. Transport effects of γ-rays become more important and the escape probability is increased. This leads to a fast, early rise and a value of $\alpha < 1$, where α is the ratio between the luminosity and the instantaneous energy generation rate by radioactive decays at maximum. In normal SNe Ia, the Δm_{15} relation can be understood as a consequence of the temperature dependence of the opacity in combination with $\alpha > 1$. As discussed in Section 2, more ^{56}Ni causes higher luminosities and temperatures. Higher temperatures lead to larger opacities and therefore, a slower drop of the luminosity from the typical value of $\approx 1.2\times$ the instantaneous energy input rate at maximum, to the instantaneous energy input rate at later times. Accordingly, for SN 2001ay with $\alpha \approx 0.55$, the LC approaches the instantaneous energy input rate from below which explains the unusually slow decline. Within our models and as a corollary, we expect that there exists a sub-class of supernovae which obeys an anti-Phillips relation. As discussed below, this sub-class should be rare.

The unusually broad spectral features can be understood by the overall shift of the overall element pattern to higher

velocities. However, this pattern remains similar to that found in normal SNe Ia (Figure 2). We demonstrated the power and sensitivity of spectral analysis. High sensitivity demands a consistent treatment with the explosion and LC models. Otherwise, even valid models may be rejected because of poor fits. However, since a good overall fit is achieved with a consistent treatment, individual features are a powerful tool to study details of the explosion physics.

We have shown that limiting the mixing during the pulsation to small scales produces a very similar abundance pattern to the one produced in standard DD models which have been shown to reproduce the observables for the majority of SNe Ia. PDD may be a promising mechanism for the DDT.

While our model fits the basic observed features of SN 2001ay, we do not mean to imply that other models are not possible. In particular, a DD model including three-dimensional effects as discussed above with a high central C/O ratio may also be a viable model and there may exist other models that fit the observed trends. Pursuing other explanations is beyond the scope of the present work.

Our model agrees reasonably well with the observations (Figure 5) but the high carbon abundance in the progenitor poses a challenge. The central region of the progenitor originates from central He burning in stars with less than 7–8 $M_{\odot}$ (Becker & Iben 1980). During the early stages of central He burning, high carbon abundances are produced by $^{4}\mathrm{He}(2\alpha,\gamma)^{12}\mathrm{C}$ burning. With time, the helium abundance is reduced in the core. Then, $^{12}\mathrm{C}(\alpha,\gamma)^{16}\mathrm{O}$ depletes ^{12}C to a typical value of 10%–25% (Umeda et al. 1999; Domínguez et al. 2001). The final amount of $^{12}\mathrm{C}/^{16}\mathrm{O}$ depends on the mass of the progenitor, and the $^{12}\mathrm{C}(\alpha,\gamma)^{16}\mathrm{O}$ rate (Buchmann 1997), and the amount chemical mixing assumed (Castellani et al. 1985; Caputo et al. 1989; Renzini & Fusi Pecci 1988; Domínguez et al. 2001). Increased chemical overshooting (or semiconvection) prolongs the phase of burning under helium depleted conditions, leading to a lower value of C/O. Although chemical overshooting prescriptions vary widely between various groups studying stellar evolution, the final outcome is a C-poor mixture. To reach high central carbon abundances, burning under He-depleted conditions must be avoided (see Straniero et al. 2003 and references therein). Straniero et al. (2003) found that they could increase the central carbon abundance somewhat by increasing mechanical overshooting. As a possible solution, we propose a common envelope phase with very strong mixing induced by a compact secondary such as a brown dwarf or planet. Common envelope evolution is generally assumed to be responsible for the formation of close binaries leading to cataclysmic variables, X-ray binaries, and supersoft-X-ray sources (Livio & Soker 1988; Ricker & Taam 2008). Moreover, close binary systems with planet or brown dwarfs have recently been detected (Neuhäuser & Posselt 2007; Hessman et al. 2011). Unfortunately, there are no systematic studies that allow one to estimate the amount of mixing. Detailed, numerical studies are few, and analytic models are insufficient to quantify the amount of chemical mixing (Meyer & Meyer-Hofmeister 1979). One observational clue may be SN 1987A, which is believed to be the result of a common envelope evolution (Podsiadlowski et al. 1990). Blue progenitors may also be a result of low metallicity (Brunish & Truran 1982; Chieffi et al. 2003), and very few SN 1987A-like events have been found (Pastorello et al. 2012; Taddia et al. 2012). Pastorello et al. (2012) estimate that SN 1987A-likes represent ∼1.5%–4% of SNe II; however, this is likely an extreme upper limit to our scenario, since the preponderance of these objects may be just from higher mass compact stars, rather than from systems in binaries that have undergone common envelope evolution. Similarly, one can use observations of WDs to provide another estimate. The number of WDs with sub-stellar companions is $\lesssim$0.5% (Farihi et al. 2005), and the number of WDs with debris disks from tidally disrupting minor planets is 1%–3% (Farihi et al. 2009). Therefore, our scenario should be quite rare, representing 0.05%–0.5% of all SNe Ia.

Finally, we want to mention the long list of limitations of our studies. We have suggested the existence of a rare sub-class of SNe Ia which should obey an anti-Phillips relation. It is up to future systematic surveys, such as LSST, to find a sufficiently large statistical sample. Note that this sub-class may be hard to separate at the bright end of SNe Ia because the decline rates for both normal and "SN 2001ay-like" supernovae are low and similar. Chemical mixing during the common envelope phase needs to be studied in detail. Our model for SN 2001ay requires a shift of the ^{56}Ni distribution and a central hole in ^{56}Ni. Although verified for a number of normal SNe Ia, late time spectra for an SN 2001ay-like are required to confirm our assumptions of little mixing. Detailed time-series of early time spectra may help to probe whether PDDs provide a common mechanism for the transition from deflagration to detonation. Detailed three-dimensional models of the pulsation phase are required to test and quantify possible mixing.

The work presented in this paper has been carried out within the NSF project "Collaborative research: Three-Dimensional Simulations of Type Ia Supernovae: Constraining Models with Observations," whose goal is to test and constrain the physics of supernovae by observations and improve SNe Ia as tools for high-precision cosmology. The project involves The University of Chicago (AST-0709181), the University of Oklahoma (AST-0707704), Florida State University (AST-0708855), Texas A&M (AST-0708873), the University of Chile in Santiago, and the Las Campanas Observatory, Chile. This research was also supported, in part, by the NSF grant AST-0703902 to P.A.H. The work of E.B. was also supported in part by SFB 676, GRK 1354 from the DFG, and US DOE Grant DE-FG02-07ER41517. I.D. has been supported in part by the Spanish Ministry of Science and Innovation project AYA2008-04211-C02-02 (I.D.). Support for Program number HST-GO-12298.05-A was provided by NASA through a grant from the Space Telescope Science Institute, which is operated by the Association of Universities for Research in Astronomy, Incorporated, under NASA contract NAS5-26555. This research used resources of the National Energy Research Scientific Computing Center (NERSC), which is supported by the Office of Science of the U.S. Department of Energy under contract no. DE-AC02-05CH11231; and the Höchstleistungs Rechenzentrum Nord (HLRN). We thank both these institutions for a generous allocation of computer time.

APPENDIX

BRIEF DESCRIPTION OF NUMERICAL METHODS

A.1. Explosion

We have calculated explosion models and LCs using the one-dimensional radiation-hydro code HYDRA using computational modules for spherical geometry (Höflich 1995, 2003a, 2003b, 2009). We solve the hydrodynamical equations explicitly by the piecewise parabolic method on 910 depth points (Colella & Woodward 1984). Because a simple α network is insufficient

Table 1
Element Yields

Element	Yield ($M_\odot$)
He	0.01
C	0.021
O	0.043
Ne	3×10^{-3}
Na	7.8×10^{-5}
Mg	1×10^{-3}
Si	0.182
P	9×10^{-5}
S	0.104
Cl	4.2×10^{-5}
Ar	0.022
K	4.8×10^{-5}
Ca	0.022
Sc	3.1×10^{-7}
Ti	1.5×10^{-3}
V	0.022
Cr	0.106
Mn	0.024
Fe	0.661
Co	1.1×10^{-3}
Ni	0.146
^{56}Ni	0.515

Notes. The yield of the stable elements at time infinity along with the total mass of ^{56}Ni produced in the explosion.

to describe in sufficient detail the chemical boundary. Nuclear burning is taken into account using an extended network of 218 isotopes from *n, p* to ^{74}Kr (Thielemann et al. 1996; Hix & Thielemann 1996; Höflich et al. 1998 and references therein). The propagation of the nuclear burning front is given by the velocity of sound behind the burning front in the case of a detonation wave. We use the parameterization as described in Domínguez & Höflich (2000). For a deflagration front at distance $r_{\rm burn}$ from the center, we assume that the burning velocity is given by $v_{\rm burn} = \max(v_t, v_l)$, where v_l and v_t are the laminar and turbulent velocities with

$$v_t = \sqrt{\alpha_T g L_f}, \tag{A1}$$

with

$$\alpha_T = (\alpha - 1)/(\alpha + 1)$$

and

$$\alpha = \rho^+(r_{\rm burn})/\rho^-(r_{\rm burn}).$$

Here, α_T is the Atwood number, L_f is the characteristic length scale, and ρ^+ and ρ^- are the densities in front of and behind the burning front, respectively. The quantities α and L_f are directly taken from the hydrodynamical model at the location of the burning front and we take $L_f = r_{\rm burn}(t)$. The transition density is treated as a free parameter. Table 1 gives the yields of the stable elements as well as the total amount of ^{56}Ni produced in the explosion.

A.2. Light Curves

From these explosion models, the subsequent expansion, bolometric, and broadband LC are calculated using monochromatic radiation transport via the Eddington Tensor method. Both the Eddington tensor and the γ-ray transport are calculated via Monte Carlo as in the three-dimensional case. We include scattering, free–free, and bound–free opacities, and include the line transitions in the Sobolev approximation. For several elements, including C, O, Mg, Si, S, Ca, Fe, Co, and Ni, we solve the statistical equations for the three main ionization stages using detailed atomic models with 10–50 super-levels with ≈12,000 transitions using the databases of Kurucz (2002) and Cunto & Mendoza (1992). The levels closest to the continuum and of other elements are treated in local thermodynamical equilibrium with about 10^6 line transitions.

A.3. Spectra

The calculations were performed using the multi-purpose stellar atmospheres program PHOENIX/1D version 16 (Hauschildt & Baron 1999; Baron & Hauschildt 1998; Hauschildt et al. 1997a, 1997b, 1996). Version 16 incorporates many changes over previous versions used for supernova modeling (Baron et al. 2007, 2006) including many more species in the equation of state (83 versus 40), twice as many atomic lines, and many more species treated in full non-LTE (NLTE) and an improved equation of state. PHOENIX/1D solves the radiative transfer equation along characteristic rays in spherical symmetry including all special relativistic effects. The NLTE rate equations for many ionization states are solved including the effects of ionization due to non-thermal electrons from the γ-rays produced by the radiative decay of ^{56}Ni, which is produced in the supernova explosion. The atoms and ions calculated in NLTE are He I–II, C I–III, O I–III, Ne I, Na I–II, Mg I–III, Si I–III, S I–III, Ca II, Ti II, Cr I–III, Mn I–III, Fe I–III, Co I–III, and Ni I–III. These are all the elements whose features make important contributions to the observed spectral features in SNe Ia. γ-ray deposition was that calculated by the LC.

Each model atom includes primary NLTE transitions, which are used to calculate the level populations and opacity, and weaker secondary LTE transitions which are included in the opacity and implicitly affect the rate equations via their effect on the solution to the transport equation (Hauschildt & Baron 1999). In addition to the NLTE transitions, all other LTE line opacities for atomic species not treated in NLTE are treated with the equivalent two-level atom source function, using a thermalization parameter, $\alpha = 0.10$ (Baron et al. 1996). The atmospheres are iterated to energy balance in the comoving frame; while we neglect the explicit effects of time dependence in the radiation transport equation, we do implicitly include these effects, via explicitly including $p\,dV$ work and the rate of gamma-ray deposition in the generalized equation of radiative equilibrium and in the rate equations for the NLTE populations.

The outer boundary condition is the total bolometric luminosity in the observer's frame. The inner boundary condition is that the flux at the innermost zone ($v = 700$ km s^{-1}) is given by the diffusion equation. Converged models required 256 optical depth points to correctly obtain the Si II λ6355 profile.

PHOENIX and HYDRA have been well tested and compared on SNe Ia (Nugent et al. 1995a, 1995b, 1997; Lentz et al. 2001; Baron et al. 2006; Höflich 2002, 2005; Höflich et al. 1998) and, in particular, compared with observed LCs and spectra of SN 1994D and SN 2001ay.

REFERENCES

Arnett, W. D. 1980, ApJ, 237, 541
Arnett, W. D. 1982, ApJ, 253, 785
Baron, E., Bongard, S., Branch, D., & Hauschildt, P. 2006, ApJ, 645, 480
Baron, E., Branch, D., & Hauschildt, P. H. 2007, ApJ, 662, 1148

Baron, E., & Hauschildt, P. H. 1998, ApJ, 495, 370
Baron, E., Hauschildt, P. H., Nugent, P., & Branch, D. 1996, MNRAS, 283, 297
Baron, E., Jeffery, D. J., Branch, D., et al. 2008, ApJ, 672, 1038
Becker, S. A., & Iben, I., Jr. 1980, ApJ, 237, 111
Brachwitz, F., Dean, D., Hix, W. R., et al. 2000, ApJ, 536, 934
Branch, D., Baron, E., Hall, N., Melakayil, M., & Parrent, J. 2005, PASP, 117, 545
Branch, D., Dang, L. C., & Baron, E. 2009, PASP, 121, 238
Bravo, E., & García-Senz, D. 2006, ApJ, 642, L157
Bravo, E., & García-Senz, D. 2009, ApJ, 695, 1244
Bravo, E., García-Senz, D., Cabezón, R. M., & Domínguez, I. 2009, ApJ, 695, 1257
Brunish, W., & Truran, J. 1982, ApJ, 49, 447
Buchmann, L. 1997, ApJ, 479, L153
Caputo, F., Tornambe, A., & Castellani, V. 1989, A&A, 222, 121
Castellani, V., Chieffi, A., Tornambe, A., & Pulone, L. 1985, ApJ, 294, L31
Chieffi, A., Domínguez, I., Höflich, P., Limongi, M., & Straniero, O. 2003, MNRAS, 345, 111
Colella, P., & Woodward, P. R. 1984, J. Comput. Phys., 54, 174
Colgate, S. A., & McKee, C. 1969, ApJ, 157, 623
Cunto, W., & Mendoza, C. 1992, Topbase Users Guide, Tech. Rep. CSC-01-92, IBM Venezuela Scientific Center, Caracas, Venezuela
Domínguez, I., & Höflich, P. 2000, ApJ, 528, 854
Domínguez, I., Höflich, P., & Straniero, O. 2001, ApJ, 557, 279
Farihi, J., Becklin, E. E., & Zuckerman, B. 2005, ApJS, 161, 394
Farihi, J., Jura, M., & Zuckerman, B. 2009, ApJ, 694, 805
Fesen, R. A., Höflich, P. A., Hamilton, A. J. S., et al. 2007, ApJ, 658, 396
Freedman, W. L., Madore, B. F., Gibson, B. K., et al. 2001, ApJ, 553, 47
Gerardy, C. L., Meikle, W. P. S., Kotak, R., et al. 2007, ApJ, 661, 995
Goldhaber, G., Groom, D. E., Kim, A., et al. 2001, ApJ, 558, 359
Goldhaber, G., & Perlmutter, S. 1998, Phys. Rep., 307, 325
Hauschildt, P. H., & Baron, E. 1999, J. Comput. Appl. Math., 109, 41
Hauschildt, P. H., Baron, E., & Allard, F. 1997a, ApJ, 483, 390
Hauschildt, P. H., Baron, E., Starrfield, S., & Allard, F. 1996, ApJ, 462, 386
Hauschildt, P. H., Schwarz, G., Baron, E., et al. 1997b, ApJ, 490, 803
Hessman, F. V., Beuermann, K., Dreizler, S., et al. 2011, in AIP Conf. Ser. 1331, Planetary Systems Beyond the Main Sequence, ed. S. Schuh, H. Drechsel, & U. Heber (Melville, NY: AIP), 281
Hix, W. R., & Thielemann, F.-K. 1996, ApJ, 460, 869
Höflich, P. 1995, ApJ, 443, 89
Höflich, P. 2002, New Astron. Rev., 46, 475
Höflich, P. 2003a, in ASP Conf. Ser. 288, Stellar Atmosphere Modeling, ed. I. Hubeny, D. Mihalas, & K. Werner (San Francisco, CA: ASP), 185
Höflich, P. 2003b, in ASP Conf. Ser. 288, Stellar Atmosphere Modeling, ed. I. Hubeny, D. Mihalas, & K. Werner (San Francisco, CA: ASP), 371
Höflich, P. 2005, Ap&SS, 298, 87
Höflich, P. 2006, Nucl. Phys. A, 777, 579
Höflich, P. 2009, in Recent Directions In Astrophysical Quantitative Spectroscopy And Radiation Hydrodynamics, ed. I. Hubeny, J. M. Stone, K. MacGregor, & K. Werner (New York: AIP), 161
Höflich, P., Gerardy, C., Fesen, R., & Sakai, S. 2002, ApJ, 568, 791
Höflich, P., Gerardy, C. L., Nomoto, K., et al. 2004, ApJ, 617, 1258
Höflich, P., & Khokhlov, A. 1996, ApJ, 457, 500
Hoflich, P., Khokhlov, A. M., & Wheeler, J. C. 1995, ApJ, 444, 831
Höflich, P., Khokhlov, A., Wheeler, J. C., et al. 1996, ApJ, 472, L81
Höflich, P., Krisciunas, K., Khokhlov, A. M., et al. 2010, ApJ, 710, 444
Höflich, P., Müller, E., & Khokhlov, A. 1993, A&A, 268, 570
Höflich, P., Wheeler, J. C., & Thielemann, F.-K. 1998, ApJ, 495, 617
Howell, A., Sullivan, M., Nugent, P. E., et al. 2006, Nature, 443, 308
Howell, D. A. 2011, Nature Commun., 2, 350
Iben, I., & Tutukov, A. 1984, ApJS, 54, 335
Ivanova, L. N., Imshennik, V. S., & Chechetkin, V. M. 1974, Ap&SS, 31, 497
Iwamoto, K., Brachwitz, F., Nomoto, K., et al. 1999, ApJS, 125, 439
Kasen, D., Röpke, F. K., & Woosley, S. E. 2009, Nature, 460, 869
Khokhlov, A. M. 1989, MNRAS, 239, 785
Khokhlov, A. 1993, ApJ, 419, L77
Khokhlov, A., Müller, E., & Höflich, P. 1992, A&A, 253, L9
Khokhlov, A., Müller, E., & Höflich, P. 1993, A&A, 270, 223
Krisciunas, K., Li, W., Matheson, T., et al. 2011, AJ, 142, 74
Kurucz, R. L. 2002, in AIP Conf. Ser. 636, Atomic and Molecular Data and Their Applications, ed. D. R. Schultz, P. S. Krstic, & F. Ownby (Melville, NY: AIP), 134
Lentz, E., Baron, E., Branch, D., & Hauschildt, P. H. 2001, ApJ, 557, 266
Lentz, E., Baron, E., Branch, D., Hauschildt, P. H., & Nugent, P. 2000, ApJ, 530, 966
Livio, M., & Soker, N. 1988, ApJ, 329, 764
Maeda, K., Benetti, S., Stritzinger, M., et al. 2010, Nature, 466, 82
Maoz, D. 2008, MNRAS, 384, 267
Maoz, D., Mannucci, F., Li, W., et al. 2011, MNRAS, 412, 1508
Maoz, D., Sharon, K., & Gal-Yam, A. 2010, ApJ, 722, 1879
Maund, J. R., Höflich, P. A., Patat, F., et al. 2010, ApJ, 725, L167
Mennekens, N., Vanbeveren, D., De Greve, J. P., & De Donder, E. 2010, A&A, 515, A89
Meyer, F., & Meyer-Hofmeister, E. 1979, A&A, 78, 167
Mochkovitch, R., & Livio, M. 1990, A&A, 236, 378
Motohara, K., Maeda, K., Gerardy, C. L., et al. 2006, ApJ, 652, L101
Neuhäuser, R., & Posselt, B. 2007, Astron. Nachr., 328, 711
Nugent, P., Baron, E., Branch, D., Fisher, A., & Hauschildt, P. 1997, ApJ, 485, 812
Nugent, P., Baron, E., Hauschildt, P., & Branch, D. 1995a, ApJ, 441, L33
Nugent, P., Phillips, M., Baron, E., Branch, D., & Hauschildt, P. 1995b, ApJ, 455, L147
Pastorello, A., Pumo, M. L., Navasardyan, H., et al. 2012, A&A, 537, A141
Penney, B., & Höflich, P. 2012, ApJ, in press
Perlmutter, S., Aldering, G., Goldhaber, G., et al. 1999, ApJ, 517, 565
Phillips, M. M. 1993, ApJ, 413, L105
Phillips, M. M., Lira, P., Suntzeff, N. B., et al. 1999, AJ, 118, 1766
Pinto, P. A., & Eastman, R. G. 2000, ApJ, 530, 757
Podsiadlowski, P., Joss, P. C., & Rappaport, S. 1990, A&A, 227, L9
Quimby, R., Höflich, P., Kannappan, S., et al. 2006, ApJ, 636, 400
Renzini, A., & Fusi Pecci, F. 1988, ARA&A, 26, 199
Ricker, P. M., & Taam, R. E. 2008, ApJ, 672, L41
Riess, A., Filippenko, A. V., Challis, P., et al. 1998, AJ, 116, 1009
Riess, A., Filippenko, A. V., Li, W., & Schmidt, B. P. 1999, AJ, 118, 2668
Ruiter, A. J., Belczynski, K., & Fryer, C. 2009, ApJ, 699, 2026
Ruiter, A. J., Belczynski, K., Sim, S. A., et al. 2011, MNRAS, 417, 408
Saio, H., & Nomoto, K. 1985, A&A, 150, L21
Saio, H., & Nomoto, K. 1998, ApJ, 500, 388
Scalzo, R. A., Aldering, G., Antilogus, P., et al. 2010, ApJ, 713, 1073
Seitenzahl, I. R., Ciaraldi-Schoolmann, F., & Röpke, F. K. 2011, MNRAS, 414, 2709
Shen, K. J., Bildsten, L., Kasen, D., & Quataert, E. 2012, ApJ, 748, 35
Silverman, J. M., Ganeshalingam, M., Li, W., et al. 2011, MNRAS, 410, 585
Straniero, O., Domínguez, I., Imbriani, G., & Piersanti, L. 2003, ApJ, 583, 878
Taddia, F., Stritzinger, M. D., Sollerman, J., et al. 2012, A&A, 537, A140
Tanaka, M., Kawabata, K. S., Yamanaka, M., et al. 2010, ApJ, 714, 1209
Taubenberger, S., Benetti, S., Childress, M., et al. 2011, MNRAS, 412, 2735
Thielemann, F.-K., Argast, D., Brachwitz, F., et al. 2003, Nucl. Phys. A, 718, 139
Thielemann, F.-K., Nomoto, K., & Hashimoto, M.-A. 1996, ApJ, 460, 408
Tutukov, A. V., & Yungelson, L. R. 1979, ACTAA, 29, 665
Umeda, H., Nomoto, K., Kobayashi, C., Hachisu, I., & Kato, M. 1999, ApJ, 522, L43
Webbink, R. F. 1984, ApJ, 277, 355
Woosley, S. E., & Weaver, T. A. 1986, in NATO ASIC Proc. 163, Nucleosynthesis and its Implications on Nuclear and Particle Physics, ed. J. Audouze & N. Mathieu (Dordrecht: Reidel), 145
Yamanaka, M., Kawabata, K. S., Kinugasa, K., et al. 2009, ApJ, 707, L118
Yamaoka, H., Nomoto, K., Shigeyama, T., & Thielemann, F.-K. 1992, ApJ, 393, L55
Yuan, F., Quimby, R. M., Wheeler, J. C., et al. 2010, ApJ, 715, 1338
Yungelson, L., & Livio, M. 1998, ApJ, 497, 168
Yungelson, L. R., & Livio, M. 2000, ApJ, 528, 108